IAC-14-B2,3,8,x26093

IMPLICATIONS OF SKY RADIANCE ON DEEP-SPACE OPTICAL COMMUNICATION LINKS

Kevin Shortt
German Aerospace Center, Germany, kevin.shortt@dlr.de

Dirk Giggenbach
German Aerospace Center, Germany, dirk.giggenbach@dlr.de

Thomas Dreischer
RUAG Schweiz AG, Switzerland, thomas.dreischer@ruag.com

Carlos Rivera
ISDEFE, Spain, crivera@isdefe.es

Robert Daddato, Andrea Di Mira, Igor Zayer
European Space Agency, Germany
robert.daddato@esa.int, andrea.dimira@eumetsat.int, igor.zayer@esa.int

As the number of deep-space missions that are turning to optical communications to support science operations increases, system designers are taking a more in depth look at the link budgets that govern such links. Noise sources, such as the radiance arising from scattering in the Earth's atmosphere and light reflected from planetary bodies in close visual proximity to spacecraft, become particularly critical given the photon-starved channels normally associated with deep-space links. In the case of the Earth's atmosphere, sky radiance becomes a significant factor when considering daytime operations especially when operators need to support spacecraft contacts close to the Sun. This paper encapsulates the implications of sky radiance on deep-space optical communication scenarios and provides an overview of the current efforts underway in Europe to further quantify its impact on future mission operations.

I. INTRODUCTION

Photons received as a result of sky radiance have a major impact on optical communication links to deep-space probes where only a handful of signal photons are received. The problem is further compounded when one wishes to support communication links with a line of sight in close proximity to the Sun.

It is important to have a good understanding of the impact of sky radiance in order to

i) apply the appropriate margins in the communications link budget;
ii) design the ground station terminal accordingly; and
iii) derive a feasible concept of operations (ConOps)

By examining the sky radiance at any given ground station site, we can optimize the amount of time that site can support a communications link and thus maximize the amount of data return from the spacecraft.

In the European context, this research is particularly timely given that the European Space Agency, as well as other European players, have set their sights on a number of deep-space missions in the coming years. These missions would benefit greatly from the advantages that optical communications systems provide in the way of maximizing the data return. In addition, this home grown research will further complement the activities already undertaken by JPL [1] and provide opportunities for future mission cross-support.

Much of the theory for today's sky radiance models was founded in the 1960's (e.g. [2]), predominantly arising from research in the military. In 1989, Eric P. Shettle wrote a seminal paper [3] weighing the pros and cons of the different aerosol models in existence at that time and highlighted their applicability to different layers of the atmosphere. Today there are a number of software packages available to model sky radiance, such as MODTRAN and libRadTran, but they all trace back to these same origins. [4][5] From a practical standpoint, efforts have been made over the years to either derive simplified databases based on the aforementioned

models [6] or real-world measurements have been analysed [7] in order to characterize sky radiance. In 2012, the Interagency Operations Advisory Group's (IOAG) Optical Link Study Group (OLSG) completed a report marking the first concerted effort to harmonize the use of free-space optical links for space missions. [8] The report contains an evaluation of the types of sensors necessary to characterize the environment surrounding an optical ground station, including sky radiance, in order to support an operational scenario.

There are certainly a number of sophisticated radiance models in existence. What is missing, however, is a simplified model that can provide first approximation of sky radiance that is suitable for selecting optical ground station (OGS) sites.

The objective of this paper is to highlight the ongoing efforts to develop such a model to support the design and deployment of a European OGS network.

II. SKY RADIANCE MODELS

Sky radiance contributes to the overall number of photons received by the detector and hence degrades the link margin. In general, there are two scattering processes at work in the atmosphere that lead to sky radiance: Rayleigh scattering and Mie scattering. Rayleigh scattering is the scattering of light from particles that are smaller than the wavelength of light being scattered (typically scattering by molecules). Mie scattering is the scattering of light from particles that are of the same magnitude in size as the wavelength of light being scattered (typically scattering by aerosols). Given the wavelengths of interest, i.e. 1064 nm and 1550 nm, Rayleigh scattering is negligible.

The characterization and, ultimately, the modelling of sky radiance is a highly complex issue and research in this field dates back to the mid-1960s when the US military was investigating the propagation of lasers through the atmosphere, in particular at optical and infrared wavelengths. Between 1964 and 1989, a number of aerosol models were developed for the purposes of general use but due to the overall complexity of the atmosphere, many fell short of this target for a variety of reasons. In a seminal paper on the subject, Eric P. Shettle [3] brought together all of the models known at the time and provided a survey of the pros and cons of each model in an attempt to consolidate the cumulative knowledge of aerosol scattering.

Shettle remarked that while some models ignored variations in the types of aerosols for different environments, others did not take into account the vertical distribution of aerosols or only examined the aerosols in the boundary layer. Nevertheless, a standard set of definitions were established along with a common approach to modelling the impact of aerosols to the propagation of EM radiation in the atmosphere.

His paper laid the groundwork for a number of modelling tools that are in use today, namely, HITRAN, LOWTRAN, MODTRAN and libRadtran. What lay at the core of Shettle's paper is a classification of aerosols, their respective sizes and their layered distribution in the atmosphere. Quantitatively, the size distributions of atmospheric aerosols are commonly represented by the following log-normal distribution [3]:

$$n(r) = \frac{dN(r)}{dr} = \sum_{i=1}^{2} \frac{N_i}{\ln(10)\, r\sigma_i \sqrt{2\pi}} exp\left[-\frac{(\log r - \log r_i)^2}{2\sigma_i^2} \right]$$

where N(r) is the cumulative number density of particles of radius r, σ_i is the standard deviation, r_i is the mode radius, and N_i is the total number for the ith mode, and the modified gamma distribution

$$\frac{dN}{dr} = n(r) = ar^\alpha exp(-br^\gamma)$$

where a, α, b and γ are parameters defining the size distribution.

Aerosol Model	Size Distribution			Type
	N_i	r_i	σ_i	
Rural	0.999875	0.03	0.35	Mixture of water soluble and dust-like particles
	0.000125	0.5	0.4	
Urban	0.999875	0.03	0.35	Rural aerosol mixtures with soot-like aerosols
	0.000125	0.5	0.4	
Maritime:				
Continental Origin	0.99	0.03	0.35	Rural aerosol mixture
Oceanic Origin	0.01	0.3	0.4	Sea salt solution in water
Tropospheric	1.0	0.03	0.35	Rural aerosol mixture

Table 1 - Representative sizes and composition for boundary layer aersols [3].

Table 1 shows typical characteristics and sizes for the boundary layer models in [3], where the size parameters refer to the log-normal size distribution.

Using the above definitions, libRadtran has the capability of generating radiance values for the atmosphere based on a single forward scattering model (i.e. light is scattered once before being received at detector). As input, libRadtran takes a text file containing a number of keywords that represent specific model parameters. The parameter of particular relevance to sky radiance is the "#aerosol" parameter, which configures the type of aerosol models based on the list of definitions above. Other keywords such as "*aerosol_haze*" and "*aerosol_default*" define the physical attributes of the aerosols such as size, shape etc. while "*aerosol_visibility*" effectively defines the concentration of aerosols by setting visibility in kilometres. For the purposes of the analysis conducted here, a series of these input files was created for different Sun zenith angles (i.e. 0°, 10°, 20°…90°) to provide a wide range of sky radiance profiles and allow for the examination of the performance of the communication link at different times during the day.

To provide an impression on radiance dependencies, three example plots based on libRadtran simulations are shown in Figure 1 for a solar zenith angle of 32°. Each of these plots represents the sky radiance at 1550 nm. "Azimuth" in those figures means "azimuth relative to direction of Sun" (i.e. 0° azimuth is pointing towards the Sun while 180° azimuth is pointing directly away from the Sun).

Figure 1 shows the difference in sky radiance for two different aerosol concentrations. Not only is there an overall increase in the amount of radiance for the high aerosol concentration (Figure 1 - top) but the presence of the Sun is more pronounced. In this particular simulation scenario, there is an order of magnitude difference in sky radiance between low and high aerosol concentrations when looking in the direction of the Sun. Additionally, in the case of the high aerosol concentration, the dependency of sky radiance on elevation significantly changes with respect to azimuth. The sky radiance profile when looking directly away from the Sun resembles that of the low aerosol case.

Combining these cases into a single closed form model would be useful for future OGS development. However, using curve-fitting tools such as MATLAB to combine all the cases is still a complex endeavour and may result in a loss of fidelity. One possible solution would be to separate these cases into non-directive scattering and forward scattering. While this method would result in

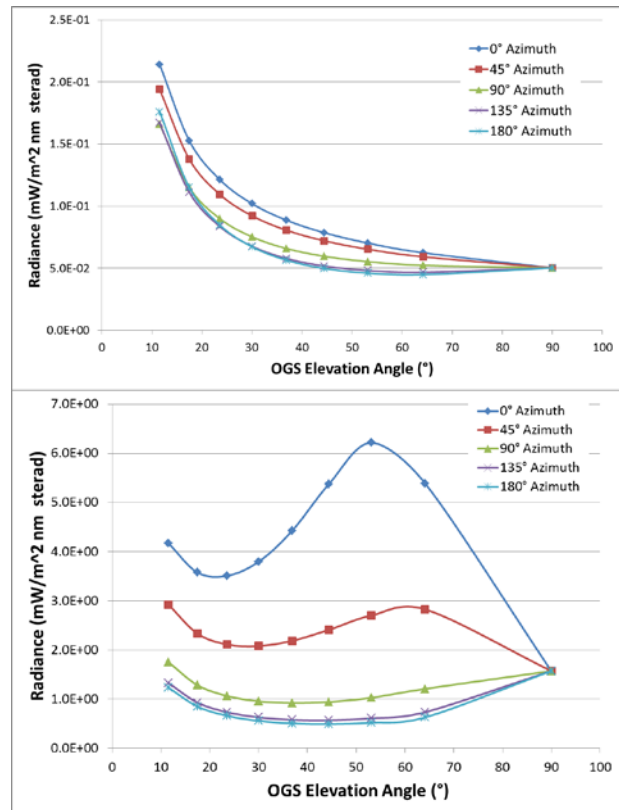two formulas, they would still be useful approximations for future OGS designers.

Figure 1 – Sky radiance for different azimuth angle for low aerosol concentration (top) and high aerosol concentration (bottom).

III. REAL-TIME CHARACTERIZATION OF SKY RADIANCE

Recent measurements of spectral sky radiance have been made at ESOC (Darmstadt, Germany) between September and December 2012. The instrument used for this purpose is a Cimel Sunphotometer: a multi–channel, automatic Sun–and–sky scanning radiometer that measures the direct solar irradiance and sky radiance at the Earth's surface. Sky measurements are taken at discrete wavelengths in the visible and near–IR parts of the spectrum during daylight hours at 440, 500, 675, 870, 1020 and 1640 nm.

The sky radiance is acquired performing two different scans called "almucantar" and "principal plane" at programmed values of airmass. For both types of scans, the instrument measures at first direct solar irradiance by pointing the collimators toward the Sun. In the almucantar configuration, the Sun–photometer keeps the zenith angle constant (equal to the solar zenith angle) and covers the whole range of discrete azimuth angle drawing an imaginary circle in the sky. In the principal

plane geometry, the azimuth angle is the one that remains constant (and equal to the solar azimuth). After pointing to the Sun, the instrument sweeps the sky in the principal plane, measuring the sky radiance at different zenith angles.

In both observation sequences, measurements are performed at a small angular interval in the region of the Sun (of the order of 1° to 2°) and at a greater interval (10° or more) away from it. A sequence of three measurements are taken creating a triplet observation per point. The scans are repeated for each of the six channels mentioned above and the entire measurement takes about 6 and 3 minutes for almucantar and principal plane, respectively. However the instrument can be programmed to measure the sky radiance at any time or airmass value. The values are automatically transferred to a computer for processing and archiving. The software provided with the instrument has been used to suppress bad measurements and derive aerosol optical depth from spectral extinction of direct beam radiation at each wavelength. To discriminate against the presence of clouds, the software executes the Smirnov et al. cloud–screening algorithm [9] based on two major criteria:

- Triplet Stability criterion: all the triplets, measured by the Sun–photometer, are compared to eliminate non–uniform scenes: only stable triplets for all the wavelengths are retained.
- Smoothness criterion: the software eliminates all the rapid temporal optical depth diurnal variations ("spikes") between selected triplets by applying a root mean square second derivative threshold, limiting sudden increase and decreases of optical depth.

The Cimel Sunphotometer is identical to those belonging to AERONET (*AErosol Robotic NETwork*), a NASA worldwide instrument network that, since the 1990s, provides reliable monitoring and archiving of global atmospheric aerosol optical and microphysical properties, to facilitate the characterization of aerosol impacts and validation of satellite products [10]. The measurements taken at ESOC between September and December 2012 were compared with the data provided by a close AERONET site (Max Plank Institute for Chemistry, Mainz), showing a very good agreement for cloud-screened sky radiance. After this preliminary validation the instrument was temporarily installed for testing in an actual ESA Ground Station (Cebreros, Spain) in June 2013 (Figure 2).
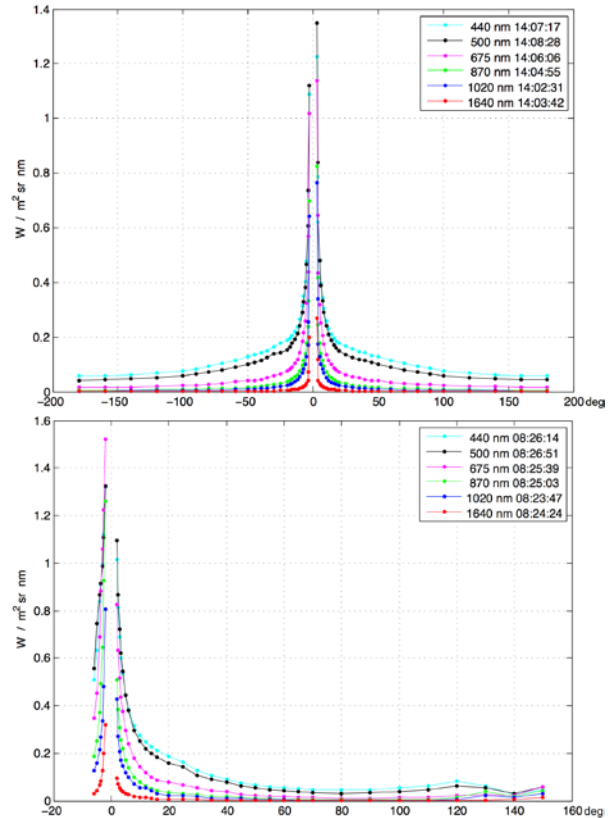

Figure 2 – Almucantar (top) and Principal Plane (bottom) radiances for the Cimel sky channels. ESA ground station of Cebreros, Spain 26/06/2013. The solar zenith angle is 27° and 52° respectively.

To further validate and integrate the measurements, a tool for sky radiance modeling was developed. The tool is based on libRadtran and the measurements taken by the Sunphotometer. As input information for the model, it is crucial to include aerosol optical properties (such as refractive index, size distribution, density and humidity) especially for simulations of sky radiance within the circumsolar region. To achieve this purpose a library based on the OPAC database [11] has been included in the software.

The resulting low root mean square error (RMSE) has led to simulate radiance at any point in the sky. This approach is of great interest because the Sun–photometer provides readings along the specific paths of almucantar and principal plane. These are used to normalize the libRadtran output profiles obtaining simulated full–sky radiance distributions.

The data provided by the Cimel Sunphotometer as well as the radiance maps would allow a significant improvement in link budget estimation in quasi real-time, based on actual measurements. On the other hand a statistical analysis of sky radiance, atmospheric transmittance and cloud coverage would support the

identification of candidate sites when designing/deploying a future optical ground station network. In this scenario a long-term data collection is fundamental to compile meaningful statistics on link availability [1][12] and AERONET is the evidence that the Sunphotometer is a valid monitoring system to achieve this goal.
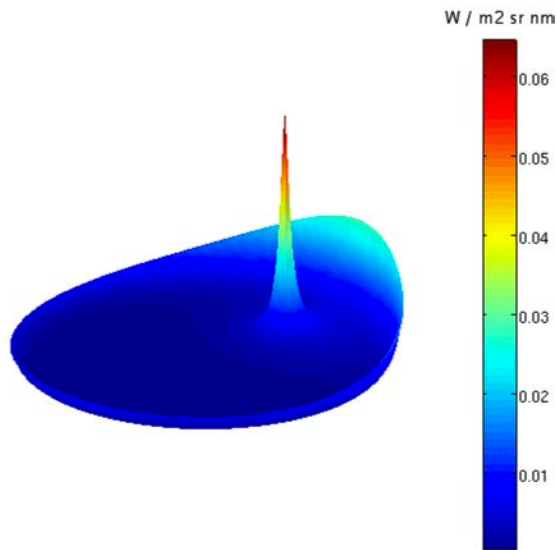

Figure 3 – Full-sky radiance distribution at 1640 nm. ESA ground station in Cebreros, Spain, 26/06/2013, 08:58 AM.

IV. DETECTOR TECHNOLOGIES TO MITIGATE IMPACT OF SKY RADIANCE

The current concept of communication systems for deep space missions is based on a direct-detection photon-counting receiver. The advantage of such a system is that it can achieve a higher channel capacity than a coherent detection system when using modulation formats with high peak-to-average power ratios. In this case, it is possible to design the receiver with a specific type of detector so that a single photon may carry an unbounded amount of information, assuming that the thermal photon contribution is negligible. This is an especially useful feature for a photon-starved channel operating under shot-noise limited conditions. However, the high photon information efficiency is achieved at the expense of reduced channel efficiency (i.e., bandwidth utilization efficiency). Moreover, practical considerations, such as peak and/or average power constraints, bandwidth constraints and the existence of dark/background noise counts, impose a finite bound on the channel capacity. The process of selecting the most suitable detector involves the examination of the channel capacity which, in turn, involves the selection of a modulation scheme that makes the most efficient use of the channel.

The proper assessment of capacity must take into account information rate, information capacity and channel efficiency. To provide some perspective from which comparisons can be drawn, it is worth noting that the ultimate information capacity for the quantum channel has been derived for the limiting case where the number of thermal photons is much higher than the average number of signal photons, applying the negentropy principle of information [13]. The resulting information capacity for a wavelength of 1550 nm and a temperature of 300 K is ≈31 bits/photon. By comparison, specific non-photon counting detection schemes such as phase insensitive (e.g., pre-amplified detection) and dual quadrature sensitive (e.g., coherent heterodyne) implementations lead to an information capacity limit of 1.44 bits/photon. Furthermore, the upper bound of the single quadrature implementation (e.g., coherent homodyne) is as high as 2.88 bits/photon.

For a signal based on coherent states, the channel capacity can be optimized using binary phase shift keying (BPSK) modulation and quantum-based receivers [14][15]. While the associated benefit of BPSK is that the peak-to-average ratio constraint is no longer applicable, the practical implementation of the optimum quantum detector is still not resolved. In addition, BPSK is most suitable for applications above the atmosphere where the transmitted signal is not affected by random wavefront phase distortions. Therefore, for direct-to-Earth deep-space downlinks, the compromise solution involves the use of pulse-position modulation (PPM), with a current bound below ≈4 bits/photon, for the direct-detection photon-counting receiver. The peak-to-average power ratio can then be optimized for a given communication scenario. Hereafter, the discussion shall focus on this latter case while considering the effect of sky radiance on the photon-counting receiver performance.

The characteristics of photon-counting detectors essentially determine the detection capabilities and limitations of the receiver. The parameters describing the general performance of these detectors include the size, the detection efficiency, the bandwidth or timing resolution, the dark count rate, the timing jitter and the dead time. The spectral range of operation is only relevant for signal purposes since the background noise rejection is addressed by an external optical filter. All parameters must be carefully considered when optimizing the communications performance. However, sky radiance mainly affects the detector performance through its temporal and saturation constraints. Under high noise background conditions, the device output may become saturated. The underlying physical mechanism depends on the processes governing the detector gain (e.g., Geiger mode operation) and the dead

time (e.g., hold-off time driven by after-pulsing) and, hence, the type of device. Basically, the arrival of successive photons in a sufficiently short period of time may lead to an indistinguishable electrical output due to signal saturation or the need to apply a recovery time. This deleterious effect can be viewed as an additional loss of detection efficiency subjected to the intensity of the flux of incident photons.

The resultant blocking may be mitigated using array architectures to reduce the density of photons per single detector (pixel), which are read out individually [16]. Figure 4 shows the blocking loss, as a measure of the efficiency of this approach, for different array structures assuming that the photon arrival follows a Poisson process and the photon density is uniformly distributed across the surface area. The use of 8×8 or larger format arrays seem sufficient to maintain the blocking loss within an acceptable level under a photon-starved regime, while the dead time is lower than the duration of the PPM symbol. Note that the interplay between symbols has not been considered for calculation purposes. The photon arrival due to background radiation in non-signal slots can lead to more stringent requirements for the arrayed solution in case that the duration of the dead time is longer than the slot width.
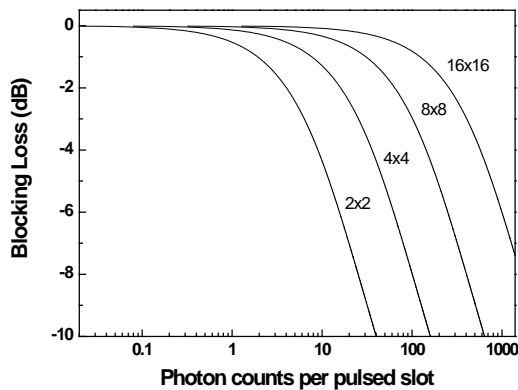

Figure 4 - Blocking loss for different array formats.

Even though other detector parameters are not so closely related to the effect of sky radiance, it is convenient to mention that slight dependencies can be identified. For example, the increase of detection efficiency is beneficial to improve channel capacity, especially under noise background limiting conditions, due to the dependence of capacity on the signal-to-noise ratio.

A more relevant issue appears when the variation of the Fried parameter (r_0) with atmospheric conditions is taken into account. It is known that seeing-limited conditions give rise to a focal spot proportional to the

ratio between the effective aperture diameter D of the receiver and r_0 instead of the simple diffraction limit. Therefore, the power collected by the detector depends on atmospheric conditions unless sufficient size is considered for the worst r_0 condition. However, if the detector size is optimized to operate in the worst condition, unnecessary noise background will be collected for larger r_0 values. In order to show the importance of this effect, calculations were performed assuming a representative case for operation at 1550 nm and 1.5 photons/bit, where D=10 m, the focal ratio F=2, a PPM order of M=64 and a slot width of 1 ns. The theoretical model assumes that the optical transfer function is that of an annular light collection system (obscuration ratio of 0.2) and Kolmogorov turbulence for long exposure image. The collected power is significantly decreased for the smaller detector (i.e., the smaller detector radius r_{Det}) designed for operation under good seeing conditions.
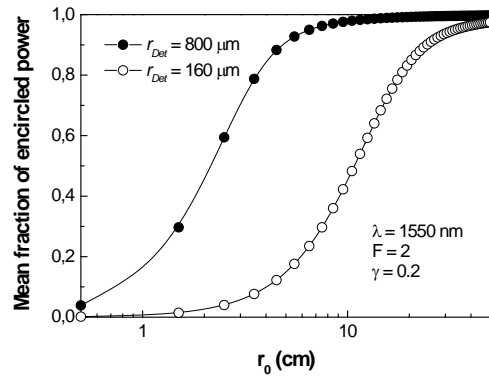

Figure 5 - Comparison of the mean fraction of encircled power for two detectors of different size as a function of r_0.

In a diffraction limited system, the image formed at the focal plane is not an actual spot but rather a spot surrounded by series of concentric rings. This pattern is known as the Airy disc and it is a mathematical precept that 84% of the total energy is located within the radius of the central disc. Therefore, one would choose a detector size that matches the size of the central Airy disc to ensure the signal is optimally received. However, atmospheric turbulence causes the disc to distort and spread out. In this case, one needs choose the detector size to ensure the energy is optimally received for the extended disc due to a given r_0.

For each mean fraction of collected power, the maximum achievable data rate is calculated as a function of r_0 (see Figure 6). Any change in the distribution of signal photons at the focal plane results in a variation of the signal-to-noise ratio, and, consequently, the useful transmission rate. In practice, the data rate can be adjusted to the link conditions by adapting the code rate, the slot width and/or the peak-to-

average power used in the modulation. The evaluation carried out here assumes that the detector size is selected such that it collects 84% of the signal photons at a given reference r_0. Using this detector size, the maximum achievable data rate is then computed over a range of r_0 values. Note that the detector size is not constrained by technology but rather has been selected here to coincide with the radius that encircles 84% of the received power. Figure 6(a) shows the data rate for two illustrative cases.

The first case, indicated by the blue line in Figure 6(a), assumes that the average number of signal photons collected by the detector is a constant 84% of the received power. To ensure this percentage of received power, the size of the detector is adapted as a function of r_0 (e.g., selecting the detection pixels of an array), thus adaptively changing the field of view for detection purposes. Noise background counts are scaled accordingly so that noise power is proportional to $(r_{0,ref}/r_0)^2$ (in this case the reference $r_{0,ref}$ is taken at 10 cm for background noise determination purposes).

For the second case, indicated by the red line, the detector size is kept fixed in order to maintain the detected noise background counts constant throughout the calculation. Results of comparison between both cases indicate that the spatial filtering resulting from the adaptive detector size strategy allows an improvement to the system performance (see also Ref. [17]).

The results shown in Figure 6(b) reveal that the data rate is degraded faster than r_0 decreases for the smaller detector, i.e., larger detectors seem preferable for low signal-to-noise ratio conditions. In this case, both the detector size and the noise background conditions were used as parameters. Namely, the 800-μm and 160-μm detector radii r_{Det} correspond to reference r_0 values of 4 cm and 20 cm, respectively. In summary, the different spatial distribution of signal and noise background photons impinging on the focal plane can be used to mitigate the effect of sky radiance on communications performance.

Detector technologies devised for deep-space photon-counting applications include single-photon avalanche diodes (SPAD) and related devices, photomultiplier tubes (PMT), intensified photodiodes (IPD), and superconducting nanowire single-photon detectors (SNSPD). If the operation is restricted to the 1.55-μm wavelength range, the main candidate technologies are currently advanced InGaAs/InP SPADs based on controlled sub-Geiger operation, InGaAsP IPDs, Nb(Ti)N SNSPDs and electron-initiated avalanche photodiode (e-APD) based on HgCdTe [18]-[22]. Most of these technologies are in an early stage of development, so that the reported state-of-the-art performance is not routinely achieved for all device types. In particular, IPDs have been successfully tested using emulated links for deep space communications. European suppliers of novel device types are small companies or research centers. Single Quantum based in the Netherlands is a prime example of a supplier of SNSPDs. SPADs are available from several companies (e.g., Aurea Technology, ST Microelectronics, Micro Photon Devices or IDQuantique). However, advanced structures like the ones required for deep space must be developed and currently the European market is oriented towards other single-photon applications. Perhaps the best industrial position is related to the HgCdTe-based APD technology, where state-of-the-art results have been reported by large companies and research centers (e.g., Selex, Leti and Sofradir). The development of appropriate deep-space single-photon detectors could take advantage of the efforts performed for similar applications (light detection and ranging, quantum communications, imaging and spectroscopy).
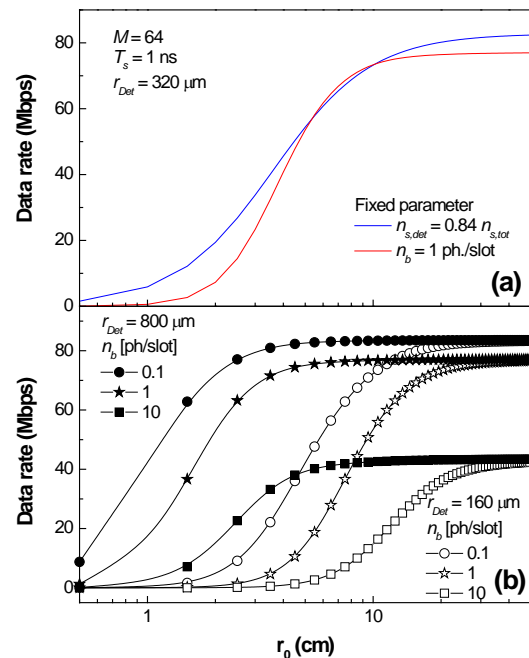

Figure 6 - (a) Data rate as a function of r_0 assuming that the number of average signal photons collected by the detector (blue line) is constant (adaptive detector size) and maintaining the noise background counts for a fixed detector size (red line). (b) Data rate for two detectors operating under three different noise background conditions as a function of r_0.

CONCLUSIONS

Sky radiance plays an important role in the design and subsequent operation of an optical ground station (OGS). This fact is particularly true when considering photon-starved direct-to-Earth deep-space communication links. As ESA, NASA and others continue to dream up exciting future deep-space missions, optical communications will become the technology of choice for delivering the vast amounts of data generated by these missions. As a consequence, a thorough understanding of the impact of sky radiance on deep-space links is required.

While there exists several sophisticated models to predict sky radiance for any location on the globe, their mere sophistication makes it difficult to generalize their results in any meaningful, yet simple, way. Real-time measurements of sky radiance require equally sophisticated processes and instrumentation for collecting and analysing the data. Streamlining such processes becomes important when developing an operational procedure for supporting daytime contacts with deep-space probes, especially when they are in close angular proximity to the Sun.

This paper has described the implications of sky radiance on deep-space optical communication scenarios and has provided an overview of the current efforts underway in Europe to further quantify its impact on future mission operations. These are both necessary steps in the development of a sky radiance model that can support the design and deployment of a European OGS network.

ACKNOWLEDGEMENTS

REFERENCES

[1] H. Hemmati, "Deep Space Optical Communications", John Wiley & Sons, 2006.

[2] E. Bell, L. Eisner, J. Young, and R. Oetjen, "Spectral Radiance of Sky and Terrain at Wavelengths between 1 and 20 Microns. II. Sky Measurements," J. Opt. Soc. Am. 50, 1313-1317, 1960.

[3] Shettle, Eric P., "Models of Aerosols, Clouds and Precipitation for Atmospheric Propagation Studies", Conf. Proc. No. 454, Atmospheric Propagation in the UV, Visible, IR and MM-wave Region and Related Systems Aspects, AGARD, October, 1989.

[4] Berk, A., Anderson, G.P, Acharya, P.K., Shettle, E.P., "MODTRAN 5.2.0.0 User's Manual", 2008.

[5] Mayer, B., Kylling, A., Emde, C., Hamann, U., Buras, R., "libRadtran User's Guide", 2012.

[6] Levoni, C., Cervino, M., Guzzi, R., Torricella, F., "Atmospheric aerosol optical properties: a database of radiative characteristics for different components and classes", Applied Optics, Vol. 36, No. 30, October 1997.

[7] Wojcik, G.S., Szymczak, H.L., Alliss, R.J., Link, R.P., Craddock, M.E. Mason, M.L., "Deep-space to Ground Laser Communications in a Cloudy World", Proc. of SPIE, Vol. 5892, 2005, doi: 10.1117/12.615435.

[8] Schulz, K.J., Rush, J., "Optical Link Study Group Final Report", Interagency Operations Advisory Group, 2012.

[9] A. Smirnov, B. Holben, T. Eck, O. Dubovik and I. Slutsker, "Cloud– screening and quality control algorithms for the AERONET database". *Remote Sensing of Environment*, vol. 73(3), p.p. 337-349, 2000.

[10] Holben B.N., T.F. Eck, I. Slutsker, D. Tanre, J.P. Buis, A. Setzer, E. Vermote, J.A. Reagan, Y. Kaufman, T. Nakajima, F. Lavenu, I. Jankowiak, and A. Smirnov, "AERONET A federated instrument network and data archive for aerosol characterization", Rem. Sens. Environ., 66, 1-16, 1998.

[11] Hess, M., P. Koepke, and I. Schult: Optical Properties of Aerosols and Clouds: The software package OPAC, Bull. Am. Met. Soc., 79, 831-844, 1998.

[12] S. Piazzolla, F. Amoozegar, R. Cesarone, "Analysis of telescope site selection for optical Deep Space Network", IEEE Aerospace Conference, Evolving Space Communication Architectures, Big Sky, Montana, March 6, 2004.

[13] Y. Yamamoto and H. A. Haus, "Preparation, measurement and information capacity of optical quantum states", Rev. Mod. Phys., Vol. 58, No. 4, pp. 1001-1020, October 1986.

[14] B. I. Erkmen, B. E. Moision, and Kevin M. Birnbaum, "The Classical Capacity of Single-Mode Free-Space Optical Communication: A Review", IPN Progress Report 42-179, pp. 1-30, November 15, 2009.

[15] V. A. Vilnrotter and C.-W. Lau, "Quantum Detection and Channel Capacity for Communications Applications," Proc. SPIE, Free-Space Laser Communications Technologies XIV, San Jose, California, pp. 103–115, January 21–22, 2002.

[16] J. A. Mendenhall, L. M. Candell, P. I. Hopman, G. Zogbi, D. M. Boroson, D. O. Caplan, C. J. Digenis, D. R. Hearn, and R.C. Shoup, "Design of an optical photon counting array receiver system for deep space communications", Proc. IEEE, vol. 95, no. 10, pp. 2059–2069, Oct. 2007.

[17] V.A. Vilnrotter and M. Srinivasan, "Adaptive Detector Arrays for Optical Communications Receivers," IEEE Trans. Commun., vol. 50, issue 7, pp. 1091–1097, July 2002.

[18] M. A. Itzler, R. Ben-Michael, C.-F. Hsu, K. Slomkowski, A. Tosi, S. Cova, F. Zappa, and R. Ispasoiu, "Single Photon Avalanche Diodes (SPADs) for 1.5 μm Photon Counting Applications", Journal of Modern Optics, vol. 54, pp. 283–304, 2007.

[19] Z. Yan, D. R. Hamel, A. K. Heinrichs, X. Jiang, M. A. Itzler, and T. Jennewein, "An Ultra Low Noise Telecom Wavelength Free Running Single Photon Detector Using Negative Feedback Avalanche Diode", Rev. Sci. Instrum.,vol. 83, p. 073105, 2012.

[20] D. Rosenberg, A. J. Kerman, R. J. Molnar, and E. A. Dauler, "High-speed and high-efficiency superconducting nanowire single photon detector array", Opt. Express, vol. 21, No. 2, pp. 1440-1447, January 2013.

[21] M. Krainak, W. Lu, G. Yang, X. Sun, D. Sykora, M. Jurkovic, V. Aebi, K. Costello, and R. Burns, "Low- Timing-Jitter Near-Infrared Single-Photon-Sensitive 16-Channel Intensified-Photodiode Detector," in CLEO:2011—Laser Applications to Photonic Applications, OSA Technical Digest, Optical Society of America, paper CThY2, 2011.

[22] J. Rothman, E. de Borniol, K. Foubert, G. Vojetta, L. Mollard, G. Perrais, F. Salvetti, A. Kerlain, and Y. Reibel, "HgCdTe e-APDs: New perspectives in light detection from single element detectors to large area imaging focal plane arrays", Optro 2012 Symposium, Optronics in Defence and Security, 8-10 February 2012.